# Expanded View Figures

**Figure EV1.  Correlations between small RNA-seq and hydro-tRNAseq protocols, related to Fig 1.**

A    The Spearman correlations between all HEK293 tRNA quantifications, including four small RNA-seq datasets (Data ref: Flores *et al*, 2014b; Data ref: Mefferd *et al*, 2015b; Data ref: Torres *et al*, 2015b,c), four well-established tRNAseq datasets using Hydro-tRNAseq and DM-tRNAseq (Data ref: Zheng *et al*, 2015b; Data ref: Gogakos *et al*, 2017b; Data ref: Mattijssen *et al*, 2017b; Data ref: Benisty *et al*, 2019b), and one previously published quantification from small RNA-seq data by Zhang *et al* (2018). The scatter plots are square-root-normalized for better visualization.

B    Principal component analysis (PCA) and linear discriminant analysis (LDA) of all absolute tRNA quantifications of HCT116, HELA, HEK293, and BJ fibroblasts, both from small RNA-seq and from Hydro-tRNAseq data. On the left, the first component of the PCA (method-related) explains 31.59% variance and the second component (cell-line-related) explains 30.83% variance. On the right, the first component of the LDA separates completely all four cell lines, regardless of the method.
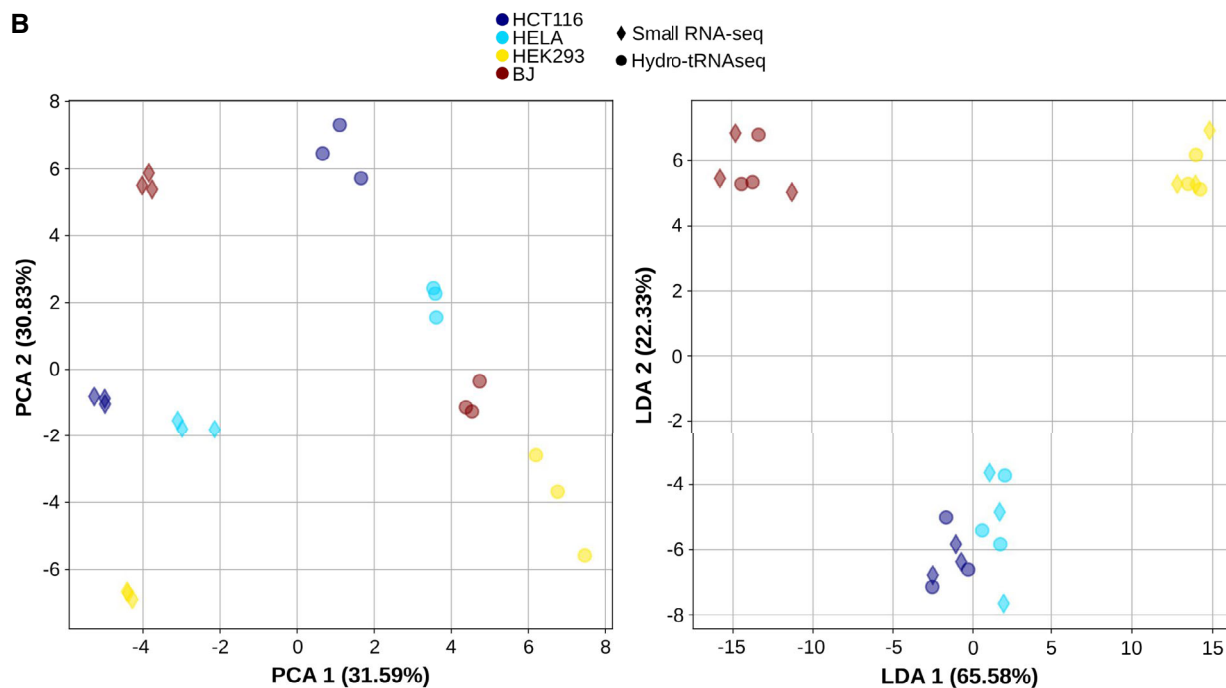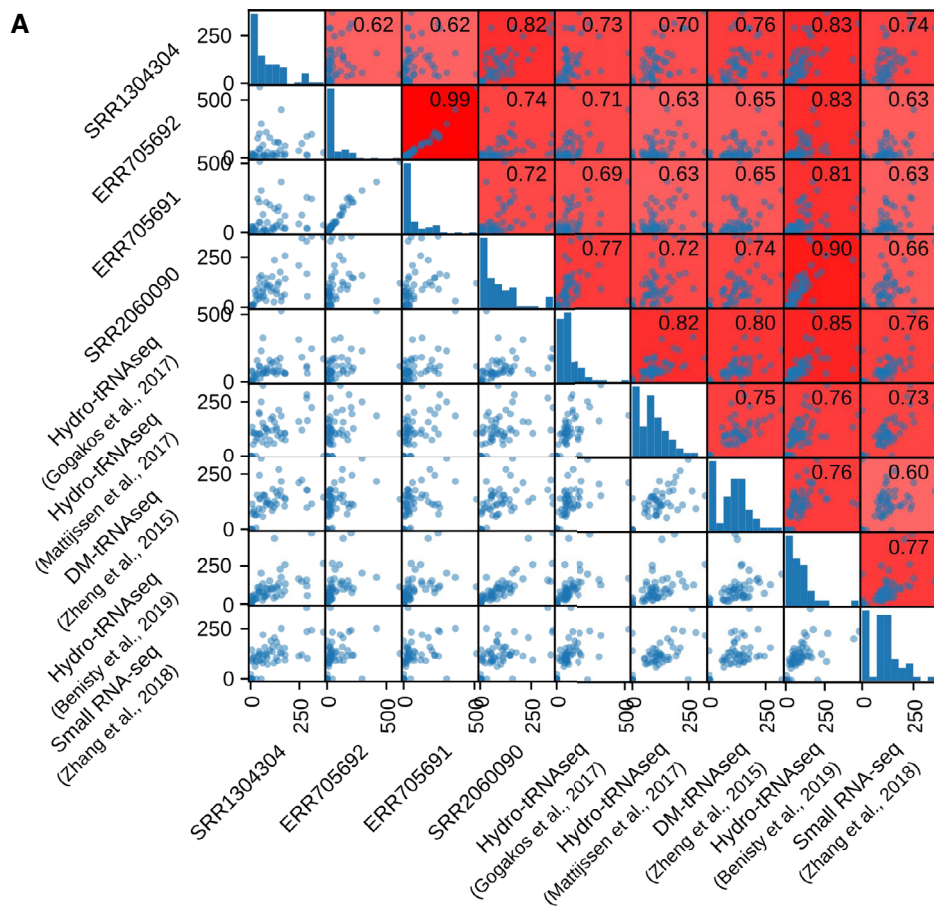
**Figure EV1.**

**Figure EV2.   Comparison between raw sequencing data from small RNA-seq (left) and Hydro-tRNAseq (right), related to Fig 1.**

A   Length distribution of all reads mapping to tRNA genes.
B   Fraction of the tRNA sequence that is covered by 1 or more reads, for each of the tRNA isoacceptors.
C   Absolute number of reads mapping along the sequence of tRNAPro$^{AGG}$. The relative abundance between cell lines is not comparable given their different sequencing depths.
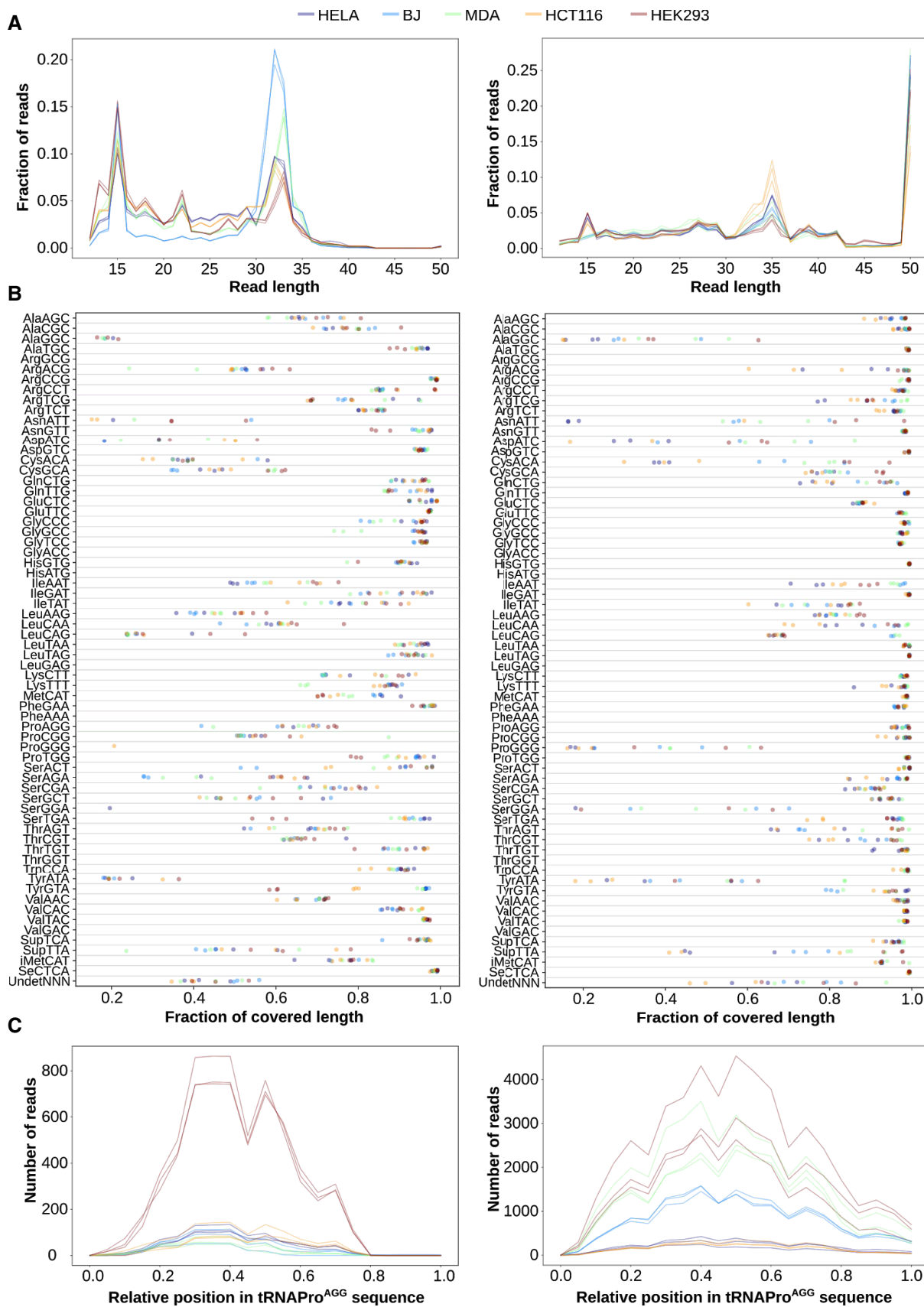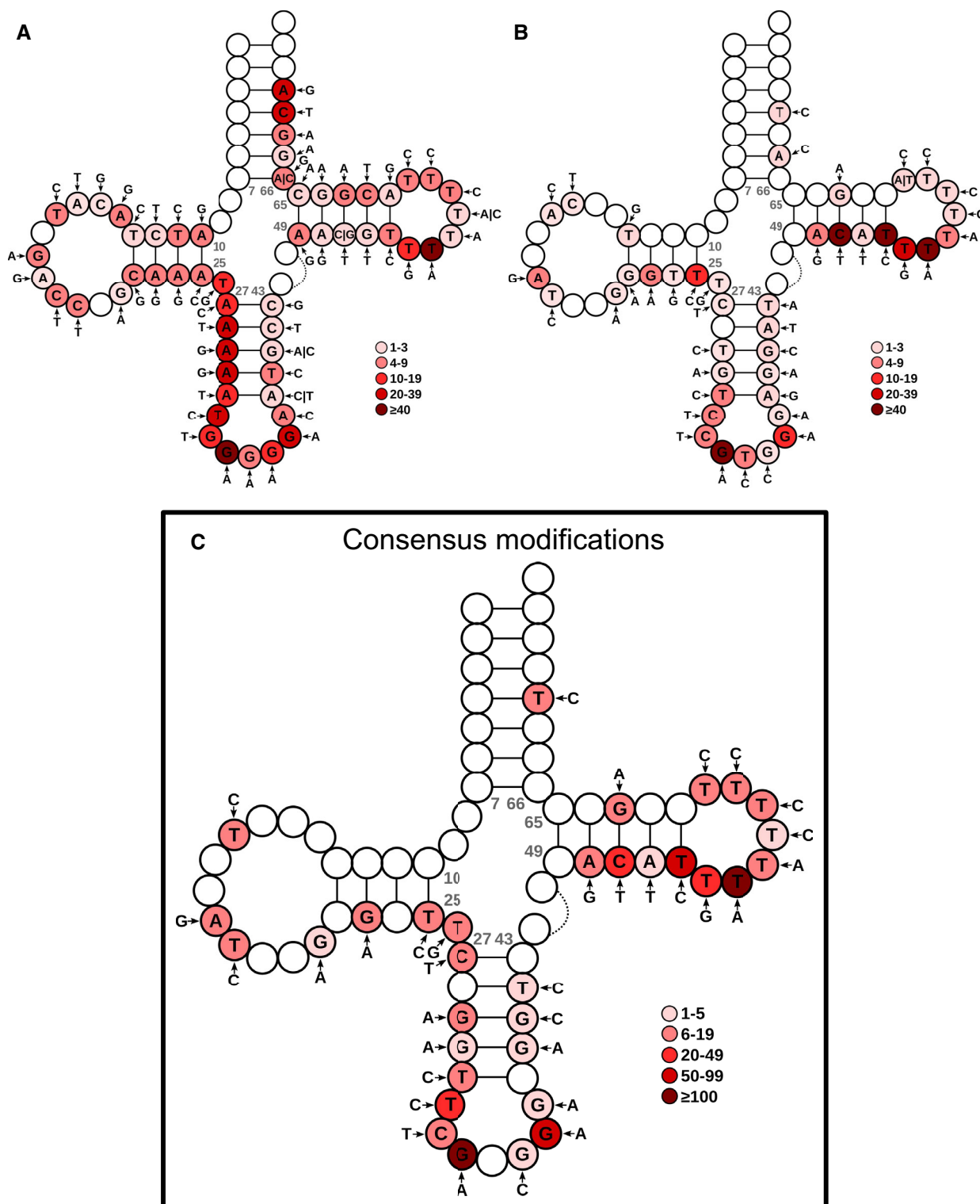
**Figure EV2.**

**Figure EV3. Nucleotide modifications of HEK293 on the consensus tRNA structure, related to Fig 1.**

A, B   Over the consensus mature tRNA structure of tRNAdb (Jühling *et al*, 2009), the most frequent detected variants are depicted for both Hydro-tRNAseq (A) and small RNA-seq (B). The color code represents the number of tRNAs showing the modification at each specific position of the tRNA model.

C   Consensus modifications detected by both methods. The color intensity refers to the sum of mismatch calls of the two methods altogether. Refer to Table EV3 for a detailed list of modifications for all cell lines.

**Figure EV4. Supply-to-Demand Adaptation across TCGA samples, related to Fig 3.**

A   Scatter plots against the proteome of the breast cancer sample TCGA-A2-A0T2-01A. Three metrics of translational efficiency (the classical tAI, a relative tAI with normalized weights within each amino acid family, and the Supply-to-Demand Adaptation described in this article) are plotted against two proxies of translation (protein abundance and protein-to-mRNA ratio). Pearson's correlation is only determined for protein abundance, since the assumption of normality is not fulfilled by the ratios.

B   Pearson's correlations of all samples for which proteomics data are available (BRCA, COAD and READ). Center values represent the median. Statistical differences are determined by sample-paired two-tailed Wilcoxon rank-sum test ($n$ = 219).

C   Medians of Supply-to-Demand Adaptation weights (SDAw) across all TCGA tissues. The dendrograms show a hierarchical clustering among tissues (right) and among SDAw (top). The tissue labels correspond to the average Ki67 expression. Refer to Table EV4 for full cancer type names and number of samples.
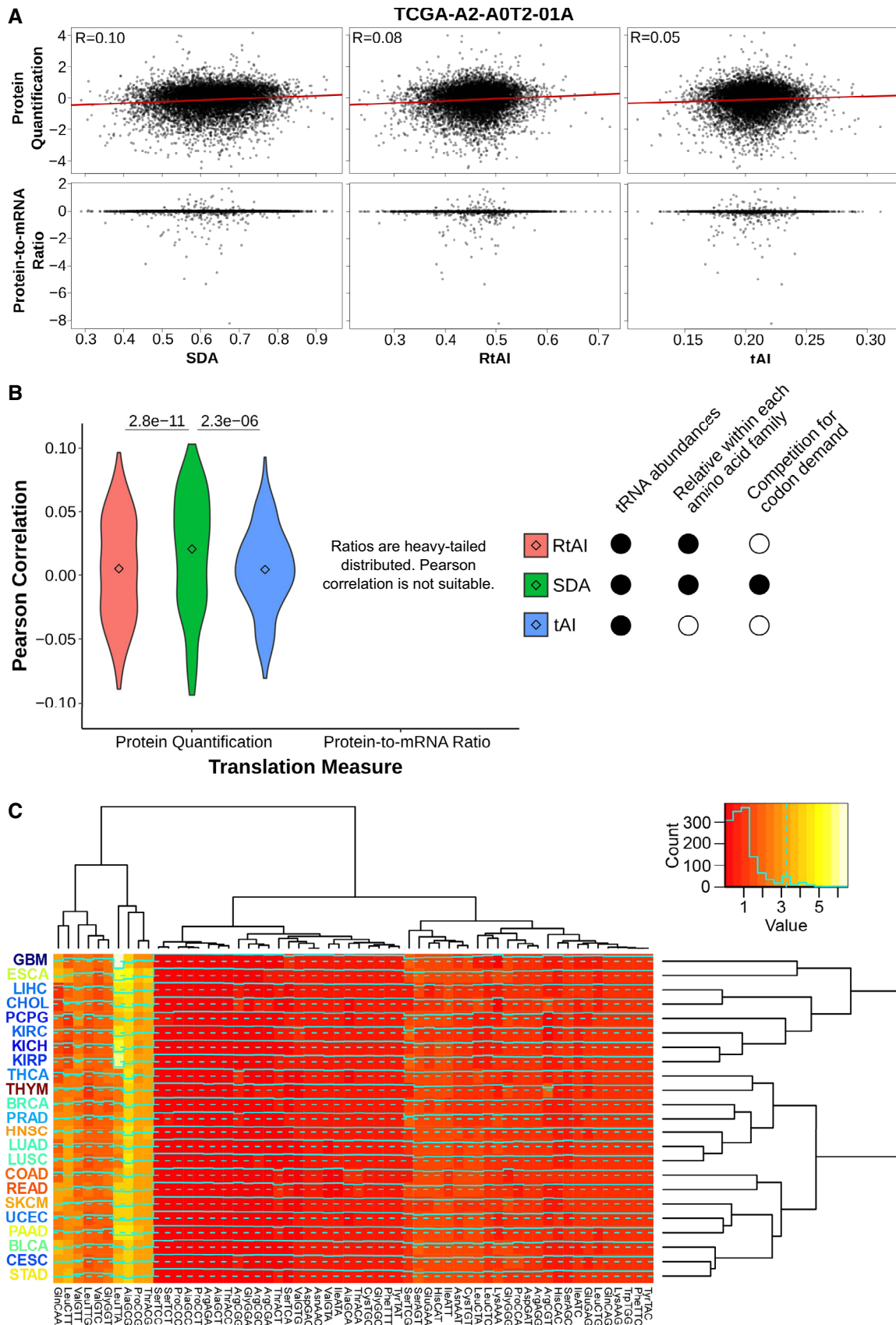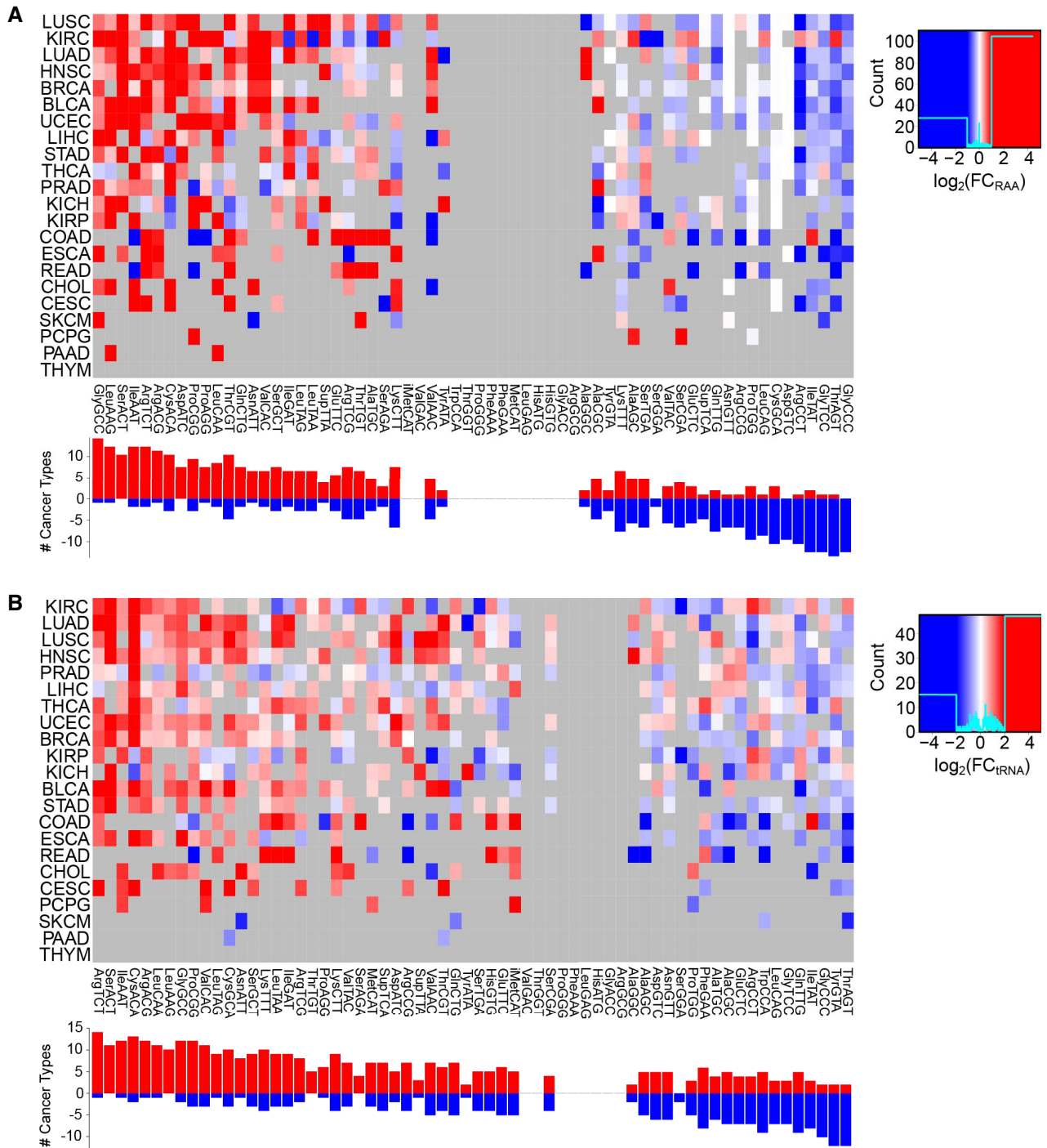
**Figure EV4.**

**Figure EV5. Differential expression of tRNAs between healthy and tumor samples across 22 cancer types, related to Fig 4.**

A   tRNA abundance is measured as relative anticodon abundance, and the fold change is $\log_2(RAA_{Tumor}/RAA_{Healthy})$. Refer to Table EV4 for full cancer type names and number of samples.

B   Absolute tRNA differential abundance by $\log_2(tRNA_{Tumor}/tRNA_{Healthy})$. Only significant differences are colored, which are determined using a two-tailed Wilcoxon rank-sum test and corrected for multiple testing by FDR.

**Figure EV6.   Differential methylation and copy number between healthy and tumor samples of tRNA genes, related to Fig 5.**

A   Differential average methylation (bisulfite sequencing) for the isoacceptors, averaged over all genes that have a certain anticodon. The difference is measured by Δ% Me = (%Me$_{Tumor}$-%Me$_{Healthy}$). Refer to Table EV4 for full cancer type names and number of samples.

B   Differential average gene copy number for the isoacceptors, averaged over all genes that have a certain anticodon. The difference is measured by ΔCNA = (CNA$_{Tumor}$- CNA$_{Healthy}$). Only significant differences are colored, which are determined using a two-tailed Wilcoxon rank-sum test and corrected for multiple testing by FDR.

C   Differential gene copy number between healthy and tumor samples of genes expressing proline tRNAs, as measured by ΔCNA. Only significant differences are colored, which are determined using a two-tailed Wilcoxon rank-sum test and corrected for multiple testing by FDR.
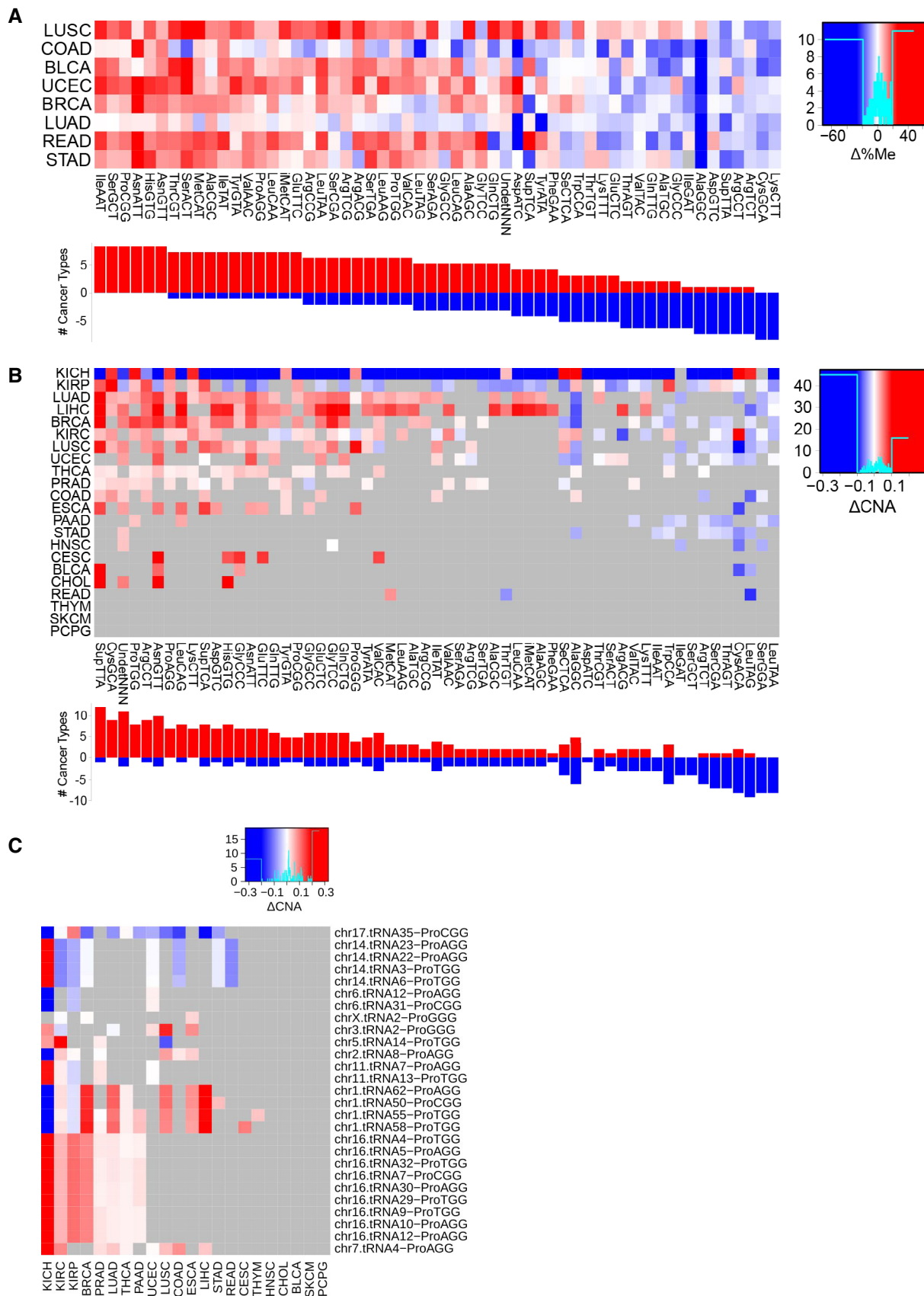
Figure EV6.